Organogels Based on PEDOT:PSS and Carbon-dots for Efficient Hole Transport in Organic Photovoltaics

Hong Chul Lim and Jong-In Hong*

Department of Chemistry, Seoul National University, Seoul 08826, Republic of Korea.
**E-mail: jihong@snu.ac.kr*
Received September 17, 2019, Accepted October 4, 2019

Keywords: Carbon-dots, PEDOT:PSS, Organogel, Hole transport, Organic photovoltaics

Organic photovoltaic devices (OPVs) have received great attention in the past decades for next-generation renewable energy sources due to the low production cost and flexible structure.[1–3] The structure of OPVs is commonly composed of anode, hole transport layer (HTL), photoactive layer, and cathode.[4–6] In general, an electrically conducting polymer such as poly(3,4-ethylenedioxythiophene)-poly(styrenesulfonate) (PEDOT:PSS) is used as the HTL to improve interfacial properties between the anode and photoactive layer.[7–9] The PEDOT:PSS consists of hydrophobic and conductive PEDOT-chains doped with hygroscopic insulator PSS, resulting in poor electrical properties.[7,9] It has been known that treatment of PEDOT:PSS with polar organic solvent or acid and annealing caused the conformational change[10–12] and thus improved the electrical conductivity.[13,14] However, controlling the orientation and shape of the PEDOT in PEDOT:PSS is still a challenge for improving the electrical percolation pathway. Recently, the electrical conductivity of PEDOT:PSS has been enhanced by inducing the gelation of PEDOT through self-assembly with graphene oxide (GO) and/or graphene quantum dots (GQDs).[15,16] Although the gelation of PEDOT:PSS improved its mechanical, thermal, and electrical properties, its morphological changes and gelation mechanism in thin films have not been well understood.

In this letter is described the development of reticulated charge–transporting networks with enhanced electrical properties of self-assembled PEDOT:PSS organogels containing carbon-dots. Carbon-dots acted as a physical linker with PEDOT-chains in PEDOT:PSS through electrostatic interactions, resulting in the formation of a core–shell (carbon-dot@PEDOT) nanostructure. Furthermore, the blending ratio of carbon-dots and PEDOT:PSS and the gelation time affected the organogel film morphology of a nanostructure which is associated with their electrical properties. The resulting carbon-dot@PEDOT:PSS organogel films were applied as an HTL for typical poly(3-hexylthiophene) (P3HT): [6,6]-phenyl-C_{61}-butyric acid methyl ester (PCBM) bulk heterojunction (BHJ) OPVs. As a result, the power conversion efficiency (PCE) of OPVs was enhanced by 30% due to the improvement of the electrical percolation pathway of the PEDOT:PSS films.

Carbon-dots were fabricated from carbon nanofibers through a hydrothermal oxidation process.[16,17] The diameter of carbon-dots was determined to be about 6 nm by high-resolution transmission electron microscopy (HRTEM) (Figure S1(a), Supporting Information). Since carbon-dots are composed of sp^2-hybridized carbon atoms, lattice images inside the carbon-dots were clearly observed (Figure S1(b)). Consequently, the quantum confinement effect of carbon-dots was expected, which was confirmed by optical properties of carbon-dots. The UV–Vis spectra of carbon-dots (0.1 wt %) in isopropyl alcohol (IPA) exhibited two peaks (Figure S2(a)). The absorption peak at 269 nm originated from the π–π^* transition of sp^2 carbon atoms in carbon-dots. The absorption peak at 347 nm was ascribed to the n–π^* transition of oxygen atoms at the edge site of carbon-dots involved in C═O and C─O groups.[18,19] Although the photoluminescence (PL) intensity was reduced with decreasing excitation energy, the PL spectra were red-shifted (Figure S2(a)). The blue PL emission at 420 nm (λ_{ex} 380 nm) was from the quantum confinement effect of carbon-dots. On the other hand, the green emission band at about 520 nm (λ_{ex} 460 nm) arises from the edge effect of oxygens.[20] Fourier-transform infrared spectroscopy (FT-IR) was performed to identify the functional groups in carbon-dots (Figure S2(b)). FT-IR exhibited a broad O─H stretching of hydroxyl groups at 3462 cm^{-1}, a C═O stretching of carboxyl groups at 1797 cm^{-1}, and C─O stretching of the epoxide ring deformation on the basal plane at 1348 and 1087 cm^{-1}. The aromatic C─C stretching was also observed at 1612 cm^{-1}.[21,22] This is consistent with the considerable generation of oxygenated functional groups at the edge sites of carbon-dots after the hydrothermal oxidation process, resulting in negatively charged carbon-dots. The surface charge of carbon-dots was measured to be −16.6 mV by a zeta potential analyzer. Thus, morphology changes were expected to occur in PEDOT:PSS through electrostatic interactions between PEDOT-chains and carbon-dots. The carbon-dots dispersed in IPA (0.5 wt %) were added to PEDOT:PSS solution. When the mixture in the vial was left undisturbed for 1 h, organogels were formed (Figure 1(a), right). However, organogels were not observed in the vial containing only PEDOT:PSS and

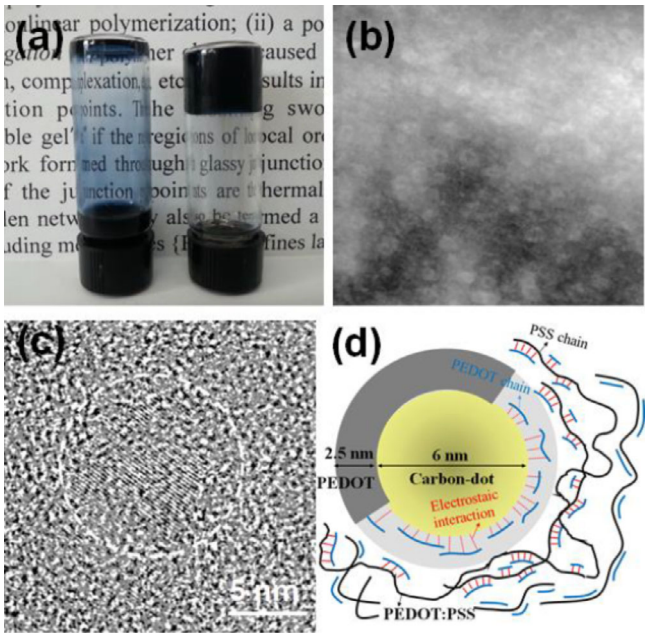

Figure 1. (a) Photography of PEDOT:PSS in IPA (left) and organogels formed with carbon-dots (right). (b) Cross-sectional high-angle annular dark-field (HAADF-STEM) image of $ogC_{0.5}$. (c) High-resolution transmission electron microscopy (HRTEM) image of a core–shell (carbon-dot@PEDOT) nanostructure. (d) Schematic representation of the core–shell nanostructure.

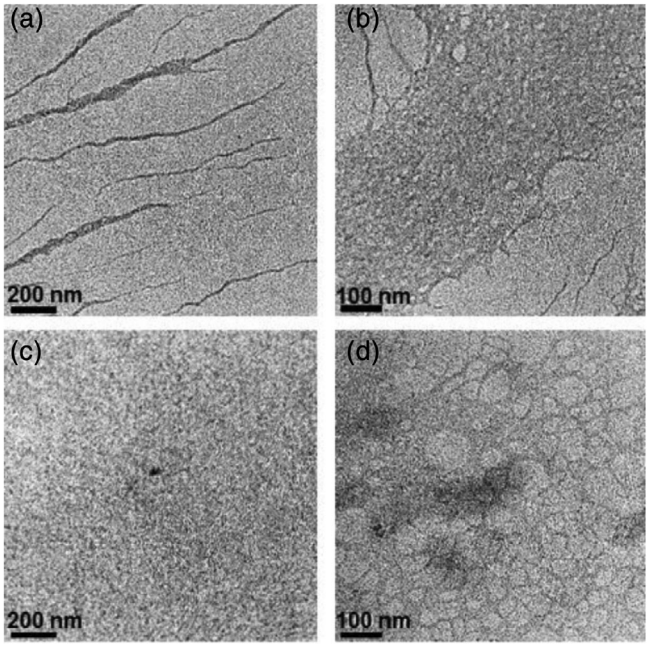

Figure 2. The sequential changes of TEM images obtained during gelation of organogel films; (a) 3 min, (b) 15 min after addition of 50 vol % carbon-dots, and (c) 3 min, (d) 15 min after addition of 20 vol % carbon-dots.

IPA without carbon-dots (Figure 1(a), left). The prepared organogels are termed as $ogC_{0.1}$, $ogC_{0.2}$, $ogC_{0.3}$, $ogC_{0.4}$, and $ogC_{0.5}$, respectively, where the subscript number refers to the volume fraction of carbon-dots (1 wt % in IPA) added to PEDOT:PSS solution. For example, $ogC_{0.5}$ indicates that the ratio of carbon-dots to PEDOT:PSS is 1:1 (v/v). The cross-sectional image of $ogC_{0.5}$ by the high-angle annular dark-field scanning TEM (HAADF-STEM) (Figure 1(b)) exhibited core–shell nanostructures with an average diameter of about 11 nm, which is 5 nm larger than that of carbon-dots. The core size almost coincides with the diameter of the as-synthesized carbon-dots. Furthermore, the lattice image of the core was revealed by HRTEM, as shown in Figure 1(c). Since the brightness of the HAADF-STEM image is proportional to the atomic number,[9] the bright shell with an average thickness of about 2.5 nm was assumed to be PEDOT-chains. Consequently, it was assumed that core–shell nanostructures are composed of carbon-dots as the core with dark images and PEDOT-chains as the shell with bright images. These results indicate that addition of a polar organic solvent such as IPA to the PEDOT:PSS solution weakened Coulomb interactions between PEDOT and PSS,[23,24] and then electrostatic interactions between positively charged PEDOT-chains and negatively charged carbon-dots resulted in core–shell (carbon-dot@PEDOT) nanostructures (Figure 1(d)). The gelation phenomena were monitored by TEM according to the concentration of carbon-dots and the gelation time. Figure 2 showed sequential changes of the TEM images depending on the concentration of carbon-dots added to the PEDOT:PSS solution and the gelation time. In the case of $ogC_{0.5}$, hyperbranched structures were observed after 3 min gelation time as shown in Figure 2(a). The hyperbranched structures then merged into interconnected structures and micro-sized reticulated features after 15 min (Figure 2(b)). On the other hand, although the hyperbranched structures were not observed in $ogC_{0.2}$ (Figure 2(c)) after 3 min, the reticulated features were also observed after 15 min (Figure 2(d)). These results indicate that the interchain interactions occurred between the core-shell nanostructures and the unreacted PEDOT-chains in PEDOT:PSS matrix during the initial state of the gelation process, resulting in the hyperbranched structures. The hyperbranched structures then merged into interconnected structures through π–π interactions and hydrogen bonding, as shown in Figure 2(b) and (d). Finally, a three-dimensionally connected self-assembled organogels were formed (Figure 1(a)).

The organogel films were used as the HTL for P3HT:$PC_{61}BM$ BHJ OPVs by the spin-coating method. The OPV performances were investigated according to the concentration and gelation time of the carbon-dots added to PEDOT:PSS solution. The characteristic parameters including an open-circuit voltage (V_{oc}), a short-circuit current (J_{sc}), a fill factor (FF), and a PCE are summarized in Table 1 and Table S1. The numbers indicated in min (Table S1) represent the gelation time between PEDOT:PSS and carbon-dots. The PCE of OPVs was enhanced with increasing gelation time in $ogC_{0.1}$ and $ogC_{0.2}$. On the other hand,

Table 1. Photovoltaic performances of BHJ OPV devices.

HTL	Control	$ogC_{0.1}$	$ogC_{0.2}$	$ogC_{0.3}$	$ogC_{0.4}$	$ogC_{0.5}$
V_{oc} (V)	11.31	14.93	15.48	13.80	14.06	14.14
J_{sc} (mA/cm^2)	0.59	0.58	0.59	0.59	0.59	0.59
FF	0.55	0.48	0.52	0.52	0.50	0.50
PCE (%)	3.67	4.15	4.78	4.21	4.11	4.15

Device configuration of ITO/HTL/P3HT:$PC_{61}BM$/LiF/Al was used in all cases.

the PCE of OPVs based on $ogC_{0.3}$, $ogC_{0.4}$, and $ogC_{0.5}$ reached maximum values at the shorter gelation time. All OPVs with organogel films as the HTL exhibited higher PCEs than control OPVs, which were prepared from the mixture of PEDOT:PSS and IPA without carbon-dots (Table 1 and Figure 3). These results support the fact that the organogel films provide a better electrical pathway for carrier hopping in HTLs, because the PEDOT-chains in the organogel films were interconnected, improving electrical properties.[13,16] Interestingly, the PCE of OPVs based on $ogC_{0.5}$ with 120 min gelation time was lower than that of the control OPVs (Table S1). This is because the excess concentration of carbon-dots and long gelation time in PEDOT:PSS interfere with the homogeneous formation of a charge transport pathway.[16] As a result, $ogC_{0.2}$ with gelation time of 90 min formed an optimum HTL to produce the highest performance OPVs.

In summary, we have developed PEDOT:PSS-based organogels containing carbon-dots as an effective HTL to enhance the hole transport in OPVs. The negatively charged carbon-dots acted as a physical linker in organogels through electrostatic interactions with the positively charged PEDOT chains in the PEDOT:PSS matrix, resulting in core–shell (carbon-dot@PEDOT) nanostructures, which affected the distribution of three-dimensionally interconnected PEDOT chains during gelation and induced the formation of organogel films. The organogel films used as the HTL significantly improved the OPV performance by up to 30%, depending on the concentration of carbon-dots and gelation time. These results suggest that the carrier transport pathway in organogel films can be improved through intermolecular interactions between carbon-dots and PEDOT:PSS, and can be applied to other optoelectronic devices such as organic light-emitting diodes and light-emitting electrochemical cells.

Experimental

Reagents and Materials. All the chemical agents used in this study were commercially available and used without further purification. Carbon nanofiber was purchased from Sigma-Aldrich (Munich, Gemany), and P3HT and $PC_{61}BM$ were purchased from Nano-C (Westwood, MA, USA). Poly (3,4-ethylenedioxythiophene)-poly(styrenesulfonate) (PEDOT:PSS, Clevios™ P) was purchased from Heraeus; (Leverkusen, Germany).

Preparation of Carbon-Dots. Carbon nanofibers (NEXCARB-H, 0.30 g) were added into a mixture of concentrated H_2SO_4 and HNO_3 (3:1 v/v), followed by sonication for 1 h and continuous stirring for 1 day at 110 °C. After cooling, the resulting solution was neutralized with Na_2CO_3. Ethanol was added to the carbon-dots solution, followed by centrifugation at 15 000 rpm for 30 min to obtain uniform-sized carbon-dots. The supernatant of carbon-dots solution was further dialyzed and dispersed into isopropyl alcohol (IPA).

Fabrication of Organic Photovoltaic Devices. The structure of the fabricated OPVs was glass/ITO/HTL/photoactive layer/LiF/Al. The HTL used was PEDOT:PSS or organogel films. The organogel films were produced by addition of carbon-dots in IPA to the PEDOT:PSS solution with various ratios from 10 to 50 vol %. The photoactive layer was P3HT:$PC_{61}BM$ blend system (1:0.8 w/w, 2 wt %) in chlorobenzene. The prepared solution was spin-coated onto the HTL and then annealed at 150 °C for 10 min in a glove box. Finally, LiF (1 nm) and Al (100 nm) as cathode were deposited under 10^{-6} Torr by thermal evaporator. The active layer was 4 mm^2.

Characterization. The optical properties were characterized by absorption (Beckman, DU650, Fullerton, CA, USA) and photoluminescence (PL) spectra (Jasco, FP-7500

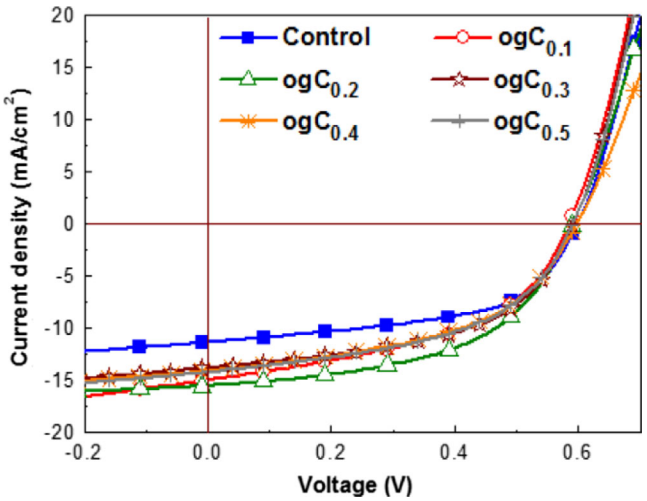

Figure 3. Current density–voltage (*J*–*V*) characteristics of the OPVs with PEDOT:PSS (control), $ogC_{0.1}$, $ogC_{0.2}$, $ogC_{0.3}$, $ogC_{0.4}$, and $ogC_{0.5}$ as hole transport layers.

spectrometer, Tokyo, Japan). The chemical composition of carbon-dots was confirmed by Fourier-transform infrared (FT-IR) spectroscopy using a Nicolet 6700 (Thermo scientific, Waltham, MA, USA). A focused ion beam (FIB, FEI Helios 650, Eindhoven, the Netherlands) was used for preparing cross-sectional samples. The thin films having less than 100 nm thickness were fabricated for TEM analysis with the lift-off method using a nanomanipulator (Omniprobe, Oxford Instruments, High Wycombe, UK). HAADF-STEM (FEI Technai F20, Eindhoven, the Netherlands) and HRTEM (JEOL JEM-2100; JEOL, Akishima, Japan) were performed to obtain cross-sectional images of organogel thin films and carbon-dots, respectively. The current density–voltage (J–V) curves were obtained using a Keithley 2400 source meter (Keithley Instruments, Solon, OH, USA) with an AM1.5 simulated white light source at 100 mW/cm^2. The active area of the device was 4 mm^2.

Acknowledgments. This work was supported by the NRF grant (No. 2018R1A2B2001293) funded by the MSIP.

Supporting Information. Additional supporting information may be found online in the Supporting Information section at the end of the article.

References

1. H. C. Lim, J.-J. Kim, J. Jang, J.-I. Hong, *New J. Chem.* **2018**, *42*, 11458.
2. R. D. Maduwu, H. C. Jin, J. H. Kim, *Macromol. Res.* **2019**, https://doi.org/10.1007/s13233-019-7174-5.
3. M. H. Hoang, G. E. Park, D. L. Phan, T. T. Ngo, T. V. Nguyen, C. G. Pakr, M. J. Cho, D. H. Choi, *Macromol. Res.* **2018**, *26*, 844.
4. J. Ko, J. Song, W. T. Choi, T. H. Kim, Y. S. Han, J. Lim, C. Lee, K. Char, *Macromol. Res.* **2018**, *26*, 623.
5. H. Heo, H. Kim, G. Nam, D. Lee, Y. Lee, *Macromol. Res.* **2018**, *26*, 238.
6. H. Cheon, Y. J. Kim, M. C. Hwang, J. Hong, T. K. An, S. K. Kwon, Y. H. Kim, *Macromol. Res.* **2018**, *26*, 29.
7. S. Kirchmeyer, K. Reuter, *J. Mater. Chem.* **2005**, *15*, 2077.
8. S. H. Roh, J. K. Kim, *Macromol. Res.* **2018**, *26*, 1173.
9. U. Lang, E. Müller, N. Naujoks, J. Dual, *Adv. Funct. Mater.* **2009**, *19*, 1215.
10. J. S. Yang, S. H. Oh, D. L. Kim, S. J. Kim, H. J. Kim, *ACS Appl. Mater. Interfaces* **2012**, *4*, 5394.
11. Y. Xia, J. Ouyang, *J. Mater. Chem.* **2011**, *21*, 4927.
12. N. Kim, S. Kee, S. H. Lee, B. H. Lee, Y. H. Kahng, Y. R. Jo, B. J. Kim, K. Lee, *Adv. Mater.* **2014**, *26*, 2268.
13. N. Kim, B. H. Lee, D. Choi, G. Kim, H. Kim, J.-R. Kim, J. Lee, Y. H. Kahng, K. Lee, *Phys. Rev. Lett.* **2012**, *109*, 106405.
14. R. S. Kohlman, A. J. Epstein, *Handbook of Conducting Polymers*, Marcel Dekker, New York, NY, **1998**.
15. H. S. Dehsari, E. K. Shalamzari, J. N. Gavgani, F. A. Taromi, S. Ghanbary, *RSC Adv.* **2014**, *4*, 55067.
16. H. C. Lim, S. H. Min, E. Lee, J. Jang, S. H. Kim, J.-I. Hong, *ACS Appl. Mater. Interfaces* **2015**, *7*, 11069.
17. E. Lee, J. Ryu, J. Jang, *Chem. Commun.* **2013**, *49*, 9995.
18. D. Pan, J. Zhang, Z. Li, M. Wu, *Adv. Mater.* **2010**, *22*, 734.
19. B. Mohamed, D. Jingjing, Z. Austin, R. Chloe, F. C. Maria, *J. Environ. Sci.* **2018**, *65*, 223.
20. K. Lingam, R. Podila, H. Qian, S. Serkiz, A. M. Rao, *Adv. Funct. Mater.* **2013**, *23*, 5062.
21. P. Juan, G. Wei, K. G. Bipin, L. Zheng, R.-A. Rebeca, G. Liehui, S. Li, B. A. Lawrence, Z. Xiaobo, G. Guanhui, A. V. Sajna, A. K. Benny, A. M. Angel, H. Takuya, J.-J. Zhu, M. A. Pulickel, *Nano Lett.* **2012**, *12*, 844.
22. M. Samal, N. Barange, D.-H. Ko, K. Yun, *J. Phys. Chem. C* **2015**, *119*, 19619.
23. J.-H. Huang, D. Kekuda, C.-W. Chu, K.-C. Ho, *J. Mater. Chem.* **2009**, *19*, 3704.
24. J. Y. Kim, J. H. Jung, D. E. Lee, J. Joo, *Synth. Met.* **2002**, *126*, 311.

